Lattice gas and spin ordering on stacked triangular lattices

1992 J. Phys.: Condens. Matter 4 8105

(http://iopscience.iop.org/0953-8984/4/41/006)

J. Phys.: Condens. Matter 4 (1992) 8105–8118. Printed in the UK

Lattice gas and spin ordering on stacked triangular lattices

J N Reimers and J R Dahn

Department of Physics, Simon Fraser University, Burnaby, British Columbia, Canada V5A 1S6

Received 11 February 1992

Abstract. Mean field theory is used to determine the highest temperature ordered phases of lattice gas and spin systems on stacked triangular lattices. We include nearest neighbour repulsive or antiferromagnetic interactions and map out the ordered phases as a function of interactions out to fifth neighbours. We show that the type of stacking, ...AAA..., ...ABAB... (hexagonal close packed), ...ABCABC... (cubic closed packed), has a profound effect on the nature of the ordering. For ...ABAB... and ...ABCABC... stacking the inter-plane interactions can compound the frustration within the planes resulting in phase diagrams dominated by incommensurate order just below the critical temperature. Comparison with relevant experimental lattice gas and magnetic systems is made.

1. Introduction

Lattice gas and spin models have been used extensively in the past to describe both intercalation and magnetic systems, respectively. Intercalation is observed in a wide variety of materials, and occurs when the chemical potential μ of the intercalant can be lowered when the intercalant enters the solid (Solin 1982, Whittingham 1978). The intercalant species usually occupy specific sites that form a lattice in the host material. In a lattice gas representation of an intercalation system one considers the host as a lattice of sites that are either occupied or unoccupied. If the intercalant species interact not only with the lattice but also amongst themselves then effects such as long-range superlattice order can occur. In statistical mechanics, lattice gas models are equivalent to the Ising model of magnetism which is a lattice of spins that point either up or down. Magnetic models with vector spins (XY or Heisenberg) have no analogue in lattice gas theory.

Magnetic ordering on two-dimensional triangular lattices with nearest neighbour antiferromagnetic interactions is a well studied problem. Wannier (1950) solved the two-dimensional Ising model on a triangular lattice proving that no long-range order occurs when the nearest neighbour interaction is antiferromagnetic. Antiferromagnetic ordering on a single triangular lattice is frustrated because at least one antiferromagnetic bond on each triangle must be broken, i.e. the spins are parallel instead of antiparallel. However, when triangular lattices are stacked along the third dimension ($\hat{c}$ direction) and inter-planar interactions are non-zero, then long-range ordering can occur (Blankschtein *et al* 1984, Matsubara and Sakari 1987a, Kim *et al* 1990). Here, we show that the type of ordering depends very much on how the triangular sheets are stacked. In some cases interactions between planes can compound the frustration already present in single two-dimensional planes.

0953-8984/92/418105+14$04.50

The simplest stacking has the lattice sites in neighbouring layers directly above and below each other with no offset along the $\hat{a}$ or $\hat{b}$ directions. We call this ...AAA... stacking (see figure 1(*a*)). Stacking with every other plane shifted by $(\frac{1}{3}, \frac{2}{3})$ in fractional hexagonal coordinates is called ...ABAB... stacking. Here lattice sites in the B layers are directly over the centres of half of the A layer triangles (see figure 1(*b*)). The third common possibility is ...ABCABC... stacking with B and C layers shifted by $(\frac{1}{3}, \frac{2}{3})$ and $(\frac{2}{3}, \frac{1}{3})$, respectively (figure 1(*c*)). ...ABAB... is called hexagonal close packing and ...ABCABC... is cubic close packing in the notation of hexagonal plane packing (Ashcroft and Mermin 1976). These names can be misleading because *true* close packing occurs only when the cell constant ratio $c/a = (\frac{8}{3})^{1/2}$ and $(6)^{1/2}$ for hexagonal and cubic close packing, respectively. Most of the experimental systems we will consider do not have the ideal ratio.

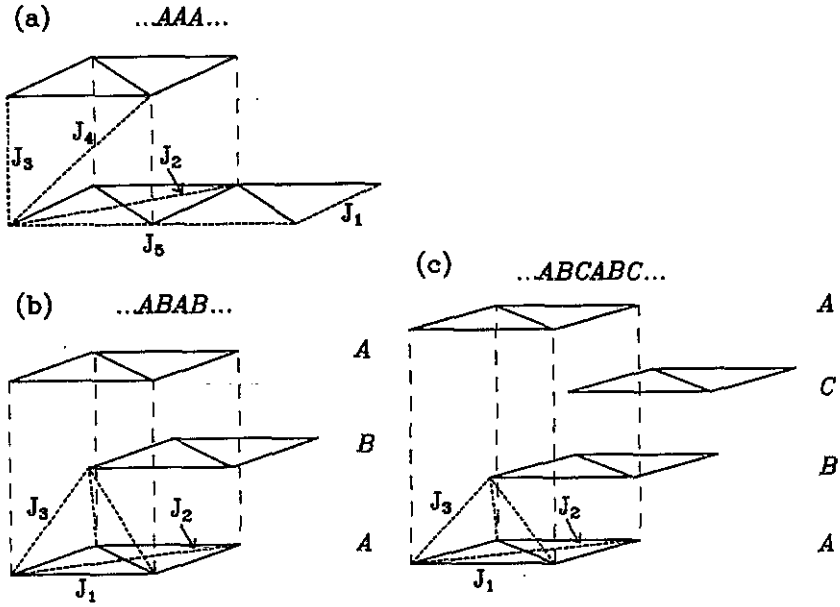

Figure 1. (*a*) A schematic picture of ...AAA...-type stacking with short broken lines indicating the five of the interactions considered. (*b*) As in (*a*) except for ...ABAB... stacking of the triangular sheets with three interactions. (*c*) As in (*a*) except for ...ABCABC... stacking of the triangular sheets with three interactions.

The goals of this work are to show that the stacking sequence profoundly affects the nature of lattice gas or magnetic ordering, and to provide insight into which interactions are necessary to stabilize a particular ordered state. A mean field theory for lattice gas systems is developed and compared to a similar theory for magnetic systems. Without any assumptions about sublattice ordering, the nature of the highest temperature ordered phases is predicted. Throughout this work the nearest neighbour interaction $J_1 < 0$ will be antiferromagnetic or repulsive. Phase diagrams in the space of the further neighbour interactions from J_2 to J_5 are calculated. The Js are defined in figure 1 for all three stacking arrangements.

We first describe the mean field theory formalism (section 2), then we discuss the phase diagrams for the three types of stacking (section 3) and finally summarize

(section 4). A comparison of the results with some experimental systems is given in section 3 for each lattice type.

2. Mean field theory

2.1. Lattice gas mean field theory

Consider a lattice gas model with the following Hamiltonian

$$\mathcal{H} = -\tfrac{1}{2}\sum_{r,r'} t_r t_{r'} J(r-r') - \mu \sum_r t_r \tag{1}$$

where r is a lattice vector, $t_r = \{0,1\}$, depending on whether lattice site r is occupied or unoccupied, $J(r-r')$ is the interaction potential between sites r and r' and μ is the chemical potential.

Here $J < 0$ and $J > 0$ correspond to repulsive and attractive interactions, respectively. We will only consider interactions that extend out to the first few coordination shells. μ has contributions from the local site potential in the lattice and secondly, in the case of electrochemical cells, from an externally applied voltage $V = -e\mu$ (McKinnon and Haering 1983). The free energy can be expressed as (with $k_B = 1$)

$$F(T,\mu) = \mathrm{Tr}(\rho\mathcal{H}) + T\,\mathrm{Tr}(\rho \ln \rho) \tag{2}$$

where ρ is the full density matrix. Within the mean field approximation, ρ is approximated as a product of single-site density matrices

$$\rho(\{t\}) = \prod_r \rho(t_r). \tag{3}$$

Following the procedure of Harris *et al* (1984) we minimize $F(T,\mu)$ with respect to $\rho_r = \rho(t_r)$ subject to the constraints that ensure normalization and keep the internal energy fixed

$$\mathrm{Tr}(\rho_r) = 1 \tag{4a}$$

$$\mathrm{Tr}(\rho_r t_r) = x_r \tag{4b}$$

where x_r is the average occupancy of site r, obtaining

$$(\partial/\partial\rho_r)\,\mathrm{Tr}\,[T\rho_r \ln \rho_r - \rho_r(\lambda_r + \mu_r t_r)] = 0 \tag{5}$$

where λ_r and μ_r are Lagrange multipliers for the constraints (4*a*) and (4*b*), respectively. From (4) and (5) one immediately determines

$$\rho_r = \exp(\beta\mu_r t_r)/[1 + \exp(\beta\mu_r)] \tag{6}$$

where μ_r can be interpreted as a local chemical potential for site r and $\beta = 1/T$. From (4*b*) and (6) we find

$$x_r = \mathrm{Tr}(\rho_r t_r) = 1/[1 + \exp(-\beta\mu_r)]. \tag{7}$$

Substituting (6) and (7) into (2) one obtains the mean field approximation to the free energy

$$F(T,\mu) = -\tfrac{1}{2}\sum_{r,r'} x_r x_{r'} J(r-r') - \mu\sum_r x_r + T\sum_r [x_r \ln x_r + (1-x_r)\ln(1-x_r)]. \tag{8}$$

2.2. Landau expansion for lattice gases

In order to deal with equation (8) analytically it is convenient to expand the entropy term in some small parameter. In general x_r is not a small parameter so we express x_r in terms of a uniform component x and a non-uniform component η_r:

$$x_r = x + \eta_r \tag{9}$$

where

$$\sum_r \eta_r = 0. \tag{10}$$

Combining (8), (9) and (10):

$$F(T,\mu) = -\frac{1}{2}\sum_{r,r'}(x^2 + \eta_r\eta_{r'})J(r-r') - \mu x + T\sum_r \left(x\ln x + (1-x)\ln(1-x) + \frac{1}{2}\eta_r^2 \frac{1}{x(1-x)} + \frac{1}{6}\eta_r^3 \frac{2x-1}{x^2(1-x)^2} + \frac{1}{12}\eta_r^4 \frac{1-3x+3x^2}{x^3(1-x)^3} + O(\eta^5)\right). \tag{11}$$

In order to diagonalize the second-order term in η, we express η_r in terms of its Fourier transform

$$\eta_r = \sum_q{}' \eta_q \exp(iq\cdot r) \tag{12}$$

where the prime on the summation symbol indicates that $q = 0$ is not included in the summation (this is necessary to satisfy (10)). In order for η_r to be real we must have

$$\eta_{-q} = \eta_q^*. \tag{13}$$

Substituting (12) into (11) we obtain

$$F/N = f(T,\mu) = \mu_0(x) + \frac{1}{2}\sum_q{}' A(x,q)\eta_q\eta_{-q} + B(x)\sum_{q_1q_2}{}' \eta_{q_1}\eta_{q_2}\eta_{-q_1-q_2} + C(x)\sum_{q_1q_2q_3}{}' \eta_{q_1}\eta_{q_2}\eta_{q_3}\eta_{-q_1-q_2-q_3} + O(\eta^5) \tag{14}$$

where

$$J_q = \sum_r J(r)\exp(iq\cdot r) \tag{15}$$

$$\mu_0(x) = -\tfrac{1}{2}x^2 J_0 - \mu x + T[x\ln x + (1-x)\ln(1-x)] \tag{16}$$

$$A(x,q) = \{T/[x(1-x)] - J_q\} \tag{17}$$

$$B(x) = (T/6)(2x-1)/[x^2(1-x)^2] \tag{18}$$

and

$$C(x) = (T/12)(1 - 3x + 3x^2)/[x^3(1-x)^3]. \tag{19}$$

Provided $A(x,q) > 0$ for all q, $f(T,\mu)$ will be minimized by $\eta_q = 0$ for all q. However, once $A(x,q) < 0$ for a single q, $f(T,\mu)$ will be minimized when that $\eta_q \neq 0$. To find the q which is selected one must examine J_q to determine for which q it is maximized. Therefore the mean field theory predicts a phase transition to an ordered phase at a critical temperature

$$T_c = x(1-x)\max_q\{J_q\}. \tag{20}$$

If the third-order term in (14) is non-zero the second-order transition predicted by (20) may be pre-empted by a first-order transition at a higher temperature. In general, the maximum of J_q is not at $q = 0$ when there are repulsive interactions and frustration.

The treatment above assumes a Bravais lattice with one site per unit cell. For ...ABAB... stacking of triangular sheets there are two sites per unit cell and Fourier transforming is insufficient to diagonalize the second-order term in (11). In this case J_q is a 2×2 matrix

$$J_q^{ab} = \sum_r J^{ab}(r)\exp(\mathrm{i}q\cdot r) \tag{21}$$

with a and b labelling the sublattices and $J^{ab}(r)$ is the interaction between two sites on sublattices a and b which are separated by r. Now the highest temperature ordered phase is determined by the maximum eigenvalue of J_q^{ab}.

2.3. Mean field theory for magnetic systems

We will consider the spin Hamiltonian with no external field

$$\mathcal{H} = -\frac{1}{2}\sum_{r,r'} J(r-r')S_r \cdot S_{r'} \tag{22}$$

where $J(r-r')$ now represents an exchange mediated interaction and S_r is a classical unit spin with n components.

$J < 0$ and $J > 0$ correspond to antiferromagnetic and ferromagnetic interactions, respectively. Three cases of physical interest are Ising ($n = 1$), XY ($n = 2$) and Heisenberg ($n = 3$). A mean field treatment similar to the one above (Reimers *et al* 1991) yields the following Landau free energy:

$$f = \frac{1}{2}\sum_q\sum_{ab} m_q^a \cdot m_{-q}^b (nT\delta^{ab} - J_q^{ab}) + \mathrm{O}(m^4) \tag{23}$$

where

$$m_q^a = \sum_r m_r^a \exp(\mathrm{i}q\cdot r) \tag{24}$$

and

$$m_r^a = \langle S_r^a \rangle. \tag{25}$$

J_q^{ab} has the same definition as before (see equation (21)). Again the highest temperature ordered phase is determined by the maximum of eigenvalue J_q^{ab}.

3. Phase diagrams

3.1. Preliminaries

In order to see the effects of further neighbour interactions in either lattice gas or magnetic systems we calculate phase diagrams in the space of $J_2/|J_1|$ and $J_3/|J_1|$. The phase diagrams are divided in regions characterized by the wavevector q that maximizes J_q. For the most part the phase diagrams were calculated by maximizing J_q numerically. Regions of incommensurate order are denoted for example by $(q,q,0)$, which indicates the direction (in this case the (110) direction) in q-space of the ordering wavevector. The ordering wavevectors reported in the diagrams are often multiply degenerate due to symmetry. For example a wavevector like (q,q,q') is actually 12-fold degenerate: $\pm(q,q,q')$, $\pm(-2q,q,q')$, $\pm(q,-2q,q')$, $\pm(q,q,-q')$, $\pm(-2q,q,-q')$ and $\pm(q,-2q,-q')$. Throughout we use the standard crystallographic representation of the hexagonal structure with the in-plane lattice vectors a and b subtending an angle of 120°, i.e. $a\cdot b = -\frac{1}{2}a^2$. The magnitude of the ordering wavevector is in general an irrational function of J_2 and J_3. A factor of 2π has been divided out of all q-vectors in figures for clarity. We must emphasize that these results only apply at temperatures just below T_c. In particular, incommensurate phases for Ising and lattice gas systems are unstable at low temperature because they do not satisfy the so-called 'hard spin' conditions

$$x_r = 0 \text{ or } 1 \qquad \text{for all } r \tag{26a}$$

or

$$|m_r| = 1 \qquad \text{for all } r. \tag{26b}$$

3.2. ...AAA... stacking

Figure 1(*a*) shows that J_2 is a second neighbour in-plane interaction and J_3 is the inter-planar interaction for this structure. We have also included a fourth neighbour interaction J_4 which may be relevant for systems with closely spaced planes. Using (15) we obtain

$$\begin{aligned} J_q = {} & 2J_1\left[\cos(q_x)+\cos(q_y)+\cos(q_x+q_y)\right] \\ & + 2J_2\left[\cos(q_x-q_y)+\cos(2q_x+q_y)+\cos(q_x+2q_y)\right] \\ & + 2J_3\cos(q_z) + 4J_4\cos(q_z)\left[\cos(q_x)+\cos(q_y)+\cos(q_z+q_y)\right]. \end{aligned} \tag{27}$$

The phase diagram for $J_4 = 0$ is shown in figure 2. The result is rather simple since the in-plane and inter-plane portions of J_q de-couple. When $J_3 < 0$, $q_z = \frac{1}{2}(2\pi)$ which means η_r or m_r alternate sign from one plane to the next. Although the sign of J_3 is important, the strength is completely irrelevant to the nature of the ordered states. When $J_2/|J_1| > -\frac{1}{8}$ three-sublattice ordering occurs ($q_x = \frac{1}{3}(2\pi)$ and $q_y = \frac{1}{3}(2\pi)$). For a lattice gas system at $x = \frac{1}{3}$, only one of the three sublattices will be occupied forming a long-range ordered state with a unit cell having dimensions $\sqrt{3}a \times \sqrt{3}a$ (see figure 3(*a*)). An analogous situation occurs at $x = \frac{2}{3}$ with two

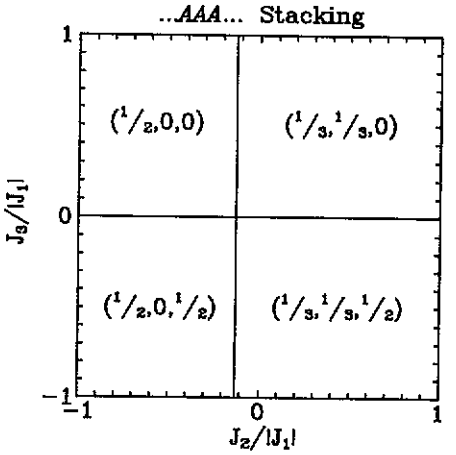

Figure 2. The phase diagram, as a function of further neighbour interactions J_2 and J_3, for the triangular lattice with ...AAA... stacking and $J_1 < 0$. Phases are characterized by their ordering wavevectors.

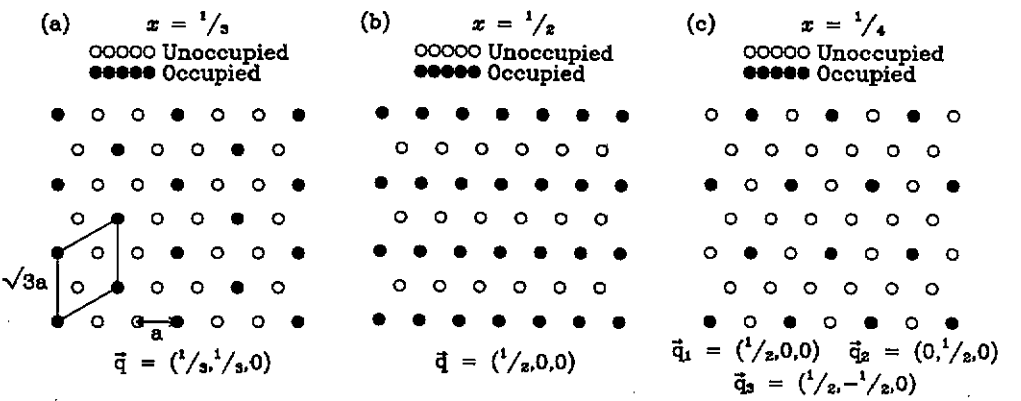

Figure 3. (*a*) The $\sqrt{3} \times \sqrt{3}$ superlattice structure for a lattice gas with wavevector $q = (\frac{1}{3}, \frac{1}{3}, 0)$ at $x = \frac{1}{3}$; an outline of the unit cell is shown. (*b*) The superlattice structure for a lattice gas with wavevector $q = (\frac{1}{2}, 0, 0)$ at $x = \frac{1}{2}$. (*c*) The superlattice structure for a lattice gas with wavevectors $q_1 = (\frac{1}{2}, 0, 0)$, $q_2 = (0, \frac{1}{2}, 0)$ and $q_3 = (\frac{1}{2}, \frac{1}{2}, 0)$, at $x = \frac{1}{4}$.

sublattices fully occupied. For Ising spins a ferrimagnetic state occurs in which each triangle has one spin up and two down, or vice versa. For vector spins a three-sublattice order occurs with each sublattice making a 120° angle with the other two, as shown in figure 4(*a*).

For $J_2 < 0$ phases with $q = (\frac{1}{2}, 0, 0)$ and $q = (\frac{1}{2}, 0, \frac{1}{2})$ are predicted. For a lattice gas system at $x = \frac{1}{2}$ this ordered state consists of alternating rows of occupied and unoccupied sites (see figure 3(*b*)). The analogous situation for spins is shown in figure 4(*b*). In general for a lattice gas problem one must consider the full range of x, $0 \leqslant x \leqslant 1$. For magnetic systems large enough fields to sample the whole range $0 \leqslant |m| \leqslant 1$ are usually experimentally inaccessible. As an example we will consider the case $q = (\frac{1}{2}, 0, 0)$ with $J_2/|J_1| = -0.5$ and $J_3/|J_1| = 0$, in detail.

There are six wavevectors in the first zone which simultaneously maximize J_q. These are $\pm(\frac{1}{2}, 0, 0)$, $\pm(0, \frac{1}{2}, 0)$ and $\pm(\frac{1}{2}, \frac{1}{2}, 0)$. Due to the constraint (13) there

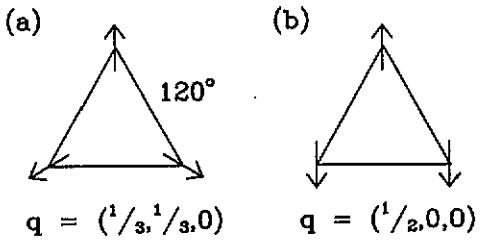

Figure 4. (*a*) The three-sublattice 120° spin structure of triangular lattice antiferromagnets with vector spins. This corresponds to a wavevector of $q = (\frac{1}{3}, \frac{1}{3}, 0)$. (*b*) As in (*a*) except for a wavevector $q = (\frac{1}{2}, 0, 0)$.

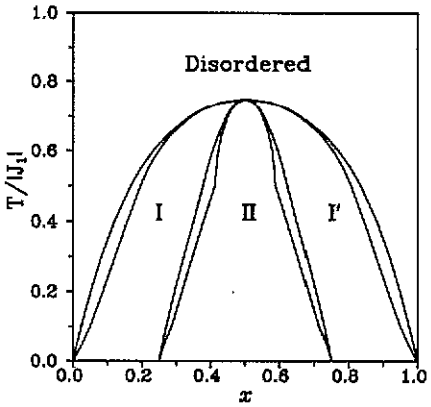

Figure 5. The mean field (x, T) phase diagram for a two-dimensional model with $J_2/|J_1| = -0.5$ and wavevector $q = (\frac{1}{2}, 0, 0)$. Phases I and II are shown in figures 3(*c*) and 3(*b*), respectively, and I' is the inverse of 3(*b*). Narrow spaces in between the labelled phases are coexistence regions for the two neighbouring phases.

are three independent order parameters, η_1, η_2 and η_3, which must satisfy

$$\eta_{q_i} = \eta_i \exp(i\phi_i) \qquad i = 1 \ldots 3 \tag{28}$$

where all η_i are real. Since only the relative phase angles ϕ_i are important we choose $\phi_1 = 0$. On substituting (28) into the Landau expansion (14) one obtains

$$f(T,\mu) = \mu_0(x) + \tfrac{1}{2}[T - T_c(x)](\eta_1^2 + \eta_2^2 + \eta_3^2) + 12B(x)\eta_1\eta_2\eta_3\cos(\phi_2 + \phi_3) + 6C(x)\left[(\eta_1^2 + \eta_2^2 + \eta_3^2)^2 + 2(\eta_1^2\eta_2^2 + \eta_2^2\eta_3^2 + \eta_3^2\eta_1^2)\right] \tag{29}$$

where $T_c(x) = 4x(1-x)|J_1|$. The product $\eta_1\eta_2\eta_3$ can always be made negative and the cosine is maximized when $\phi_2 = \phi_3 = 0$. At this point one must decide between two extreme cases for which the second-order term is invariant:

Case 1. $\eta_1 = \eta$, $\eta_2 = \eta_3 = 0$ (see figure 3(*b*)):

$$f_1(T,\mu) = \mu_0(x) + \tfrac{1}{2}[T - T_c(x)]\eta^2 + 6C(x)\eta^4. \tag{30}$$

Case 2. $\eta_1 = \eta_2 = \eta_3 = \eta/\sqrt{3}$ (see figure 3(*c*)):

$$f_2(T,\mu) = \mu_0(x) + \tfrac{1}{2}[T - T_c(x)]\eta^2 + 4/\sqrt{3}B(x)\eta^3 + 10C(x)\eta^4. \tag{31}$$

Case 2 has all three modes mixed with equal weight, which allows the third-order term. For case 1 only one mode is present and there is no third-order term. For $x < \frac{1}{2}$, $B(x)$ is negative and case 2 has a lower free energy with $\eta > 0$. The same is true for $x > \frac{1}{2}$ except now $\eta < 0$. $x = \frac{1}{2}$ is a special case with $B(\frac{1}{2}) = 0$ and f_1 and f_2 differ only in the fourth-order terms from which we see that case 1 is preferred since $C(\frac{1}{2}) > 0$.

The full (x, T) phase diagram (see figure 5) has been calculated by numerically minimizing (8) on a four-sublattice cluster which is commensurate with all of the ordering wavevectors. Phases I and II are shown in figures 3(*c*) and 3(*b*), respectively. Phase I′ is the inverse of I. The narrow areas between the labelled phases are coexistence regions.

In general, the determination of which ordering modes are selected must be done on a case-by-case basis. The third-order term can always be made negative when $x \neq \frac{1}{2}$ and if three of the ordering wavevectors can satisfy $q_1 + q_2 + q_3 = 0$ the system will select at least three of the order parameters and not just one.

For systems with small inter-planar spacings the bond distance spanned by J_2 in figure 1(*a*) may be longer than the J_4 bond distance. J_4 may also be important for other systems since there are twelve J_4 bonds and only six J_2 bonds. The phase diagram in the space of J_3 and J_4 with $J_2 = 0$ is shown in figure 6. In this case the strength of J_3 becomes important. The diagram is dominated by regions of three-sublattice order. Along the phase boundaries labelled 1 the in-plane interaction J_1 cancels with J_4, resulting in a degeneracy throughout the whole $q_z = \frac{1}{2}$ plane.

The results for ...AAA... stacking are rather simple and do not really require such sophisticated methods, the gross features of the phase diagram could be determined solely from an intuitive approach. However, as we shall see, the results for other stackings are much more complicated.

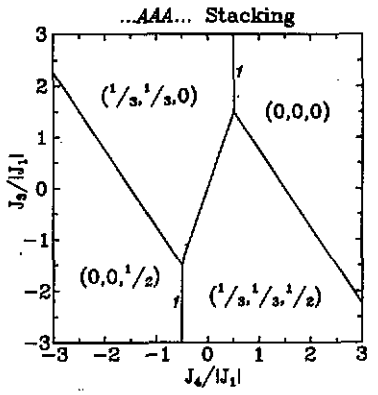

Figure 6. The phase diagram, as a function of further neighbour interactions J_4 and J_3, for the triangular lattice with ...AAA... stacking and $J_1 < 0$. Along the phase boundaries labelled 1 in the in-plane interaction J_1 cancels with J_4, resulting in a degeneracy throughout the whole $q_z = \frac{1}{2}$ plane for $J_3 < 0$ and the whole $q_z = 0$ plane for $J_3 > 0$.

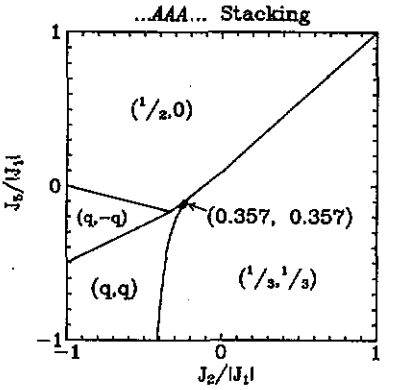

Figure 7. The phase diagram, as a function of further neighbour in-plane interactions J_2 and J_5, for the triangular lattice with ...AAA... stacking and $J_1 < 0$. The two full circles in the bottom left quadrant indicate the end points of the line (see text) where the system selects the ordering wavevector $q = 2\pi(0.357, 0.357)$, experimentally observed in $RbMnBr_3$.

The layered dichalcogenide 2H–TaS_2 is known to intercalate lithium, forming Li_xTaS_2. Ordering of the lithium ions occurs at $x = \frac{1}{3}$ and $x = \frac{2}{3}$ (Dahn and McKinnon 1984a, b), presumably with the superlattice structure shown in figure 3(*a*). $CsMnBr_3$ is a well studied stacked triangular antiferromagnet with XY spins and orders with the 120° spin structure (Eibschutz *et al* 1973). The related material $RbMnBr_3$ has the same basic crystal structure as $CsMnBr_3$;

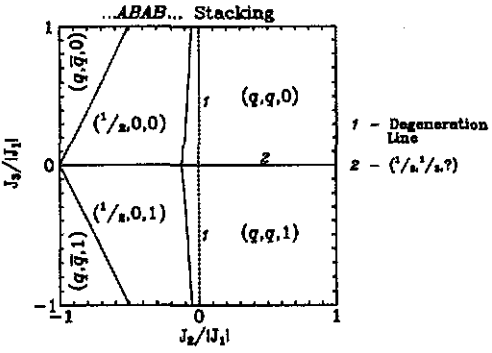

Figure 8. The phase diagram, as a function of further neighbour interactions J_2 and J_3, for the triangular lattice with ...ABAB... stacking and $J_1 < 0$. The broken line labelled 1 is not a phase boundary but indicates that J_q is maximized by an infinite number of wavevectors which form a degeneration line in the $q_z = 0$ plane. Only along the line labelled 2 does the system select the three-sublattice ordering with $q = (\frac{1}{3}, \frac{1}{3}, q_z)$.

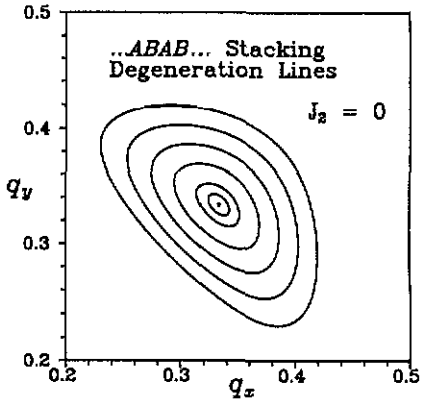

Figure 9. Degeneration lines in q-space (...ABAB... stacking) for $J_2 = 0$ and $J_3/|J_1| = 1.0$ (outer circle), 0.8, 0.6, 0.4, 0.2, 0.1 and 0.0 (the point at $(\frac{1}{3}, \frac{1}{3})$).

however, magnetic ordering in this material is incommensurate with wavevector $q = 2\pi(0.357(4), 0.357(4), 0)$ (Glinka *et al* 1973). In order to explain this within the context of mean field theory one must invoke further in-plane interactions or start with a more complicated Hamiltonian. Figure 7 shows the phase diagram as a function of J_2 and J_5 where J_5 is the in-plane interaction to the third coordination shell. Along the line $J_2/|J_1| = 0.8304J_5/|J_1| - 0.1484$ for $-0.126 \leqslant J_5 \leqslant -0.105$ the system selects the in-plane wavevector observed in $RbMnBr_3$. The two end points of the line are shown in figure 7 by full circles.

3.3. ...ABAB... stacking

The unit cell has lattice sites at $r_1 = (0,0,0)$ and $r_2 = (\frac{1}{3}, \frac{2}{3}, \frac{1}{2})$. This lattice (figure 1(*b*)) is a non-Bravais lattice and is also non-centrosymmetric, hence J_q^{ab} is an Hermitian 2×2 matrix:

$$J_q^{11} = J_q^{22} = 2J_1\left[\cos(q_x) + \cos(q_y) + \cos(q_x + q_y)\right] + 2J_2\left[\cos(q_x - q_y) + \cos(2q_x + q_y) + \cos(q_x + 2q_y)\right] \tag{32}$$

and

$$J_q^{12} = J_q^{21^*} = J_3\cos(\tfrac{1}{2}q_z)\left(e^{i(q_x+2q_y)/3} + e^{i(q_x-q_y)/3} + e^{-i(2q_x+q_y)/3}\right). \tag{33}$$

This matrix has eigenvalues

$$\lambda_q^{\pm} = J_q^{11} \pm |J_3\cos(\tfrac{1}{2}q_z)|\left\{3 + 2[\cos(q_x) + \cos(q_y) + \cos(q_x + q_y)]\right\}^{1/2} \tag{34}$$

of which λ^+ is always a maximum. The relative phases of the two sublattices are determined by the eigenvectors of J_q^{ab}. We avoid the complication of dealing with eigenvectors by selecting $q_z = 0$ for $J_3 > 0$ and $q_z = 2\pi$ for $J_3 < 0$, the second case resulting in an anti-phase relationship between the A and B layers.

The results are shown in figure 8. This phase diagram is dominated by regions of incommensurate order unlike the ...AAA... stacked lattice. Along the phase boundary labelled 2 for $J_3 = 0$, the system selects the usual three-sublattice structure with $q = (\frac{1}{3}, \frac{1}{3}, ?)$, where the question mark indicates that q_z is indeterminate because there is no inter-plane interaction. As J_3 becomes non-zero the ordering wavevector deviates continuously from $(\frac{1}{3}, \frac{1}{3}, 0)$, resulting in incommensurate long-range order. For small J_3, $q = (q, q, 0)$ and

$$\frac{q}{2\pi} = \frac{1}{3} + \frac{\sqrt{3}}{6(6J_2 + 1)}|J_3| - \frac{\sqrt{3}(12J_2 - 1)}{72(6J_2 + 1)^3}|J_3|^2 + O(|J_3|^3). \tag{35}$$

The broken line labelled 1 is not a phase boundary but represents another special situation. When $J_2 = 0$, λ_q^+ is maximized not by a single point in the zone but by an infinite number of points which form a ring in the $q_z = 0$ plane. Such lines are commonly referred to as *degeneration lines*. For $J_2 = 0$ and $q_z = 0$ we can write

$$\lambda_q^+ = 2J_1 Q + |J_3|(3 + 2Q)^{1/2} \tag{36}$$

$$Q = \cos(q_x) + \cos(q_y) + \cos(q_x + q_y). \tag{37}$$

Upon maximizing with respect to Q we obtain

$$Q = \tfrac{1}{2}(J_3/2J_1)^2 - \tfrac{3}{2}. \tag{38}$$

Solutions to (38) for various values of J_3/J_1 are shown in figure 9 and form concentric rings centred about $q = (\frac{1}{3}, \frac{1}{3}, 0)$, which increase in size as J_3 increases. Below T_c the system will be confined to a somewhat restricted phase space which includes only those Fourier modes that lie on the degeneration line. This restricted phase space will most likely result in short-range correlations but no long-range order within the mean field approximation. Thermal fluctuations beyond the mean field level may break this degeneracy and select a long-range ordered phase (Villain *et al* 1980). Matsubara and Sakari (1987b) claim that a transition to incommensurate long-range order takes place, implying that the system does select only one q-vector on the degeneration line. This may be an artifact of the finite lattice sizes for which only a discrete set of ordering wavevectors are available. Diep has shown that the system undergoes a first-order transition to long-range order for the special case $J_3 = J_1 < 0$ (Diep 1992). We are unaware of any lattice gas systems with ...ABAB... stacking but the uranium sublattice in the heavy fermion superconductor UPt_3 has this structure. Below 5 K (Aeppli *et al* 1988) antiferromagnetic order (figure 4(*b*)) sets in with propagation vector $q = (\frac{1}{2}, 0, 1)$ (Goldman *et al* 1986). This suggests a negative J_2 and J_3, as seen from figure 8.

3.4. ...ABCABC... stacking

This lattice when described in the hexagonal setting has three sites per unit cell at $r_1 = (0, 0, 0)$, $r_2 = (\frac{1}{3}, \frac{2}{3}, \frac{1}{3})$ and $r_3 = (\frac{2}{3}, \frac{1}{3}, \frac{2}{3})$. However, it is more convenient to work in the rhombohedral setting with one atom per unit cell. The lattice vectors in the two representations are related by

$$\begin{pmatrix} a \\ b \\ c \end{pmatrix}_H = \begin{pmatrix} 1 & -1 & 0 \\ 0 & 1 & -1 \\ 1 & 1 & 1 \end{pmatrix} \begin{pmatrix} a \\ b \\ c \end{pmatrix}_R . \tag{39}$$

In the rhombohedral basis

$$J_q = 2J_1\left[\cos(q_x - q_y) + \cos(q_y - q_z) + \cos(q_z - q_x)\right] + 2J_2\left[\cos(2q_x - q_y - q_z) + \cos(2q_y - q_z - q_x) + \cos(2q_z - q_x - q_y)\right] + 2J_3\left[\cos(q_x) + \cos(q_y) + \cos(q_z)\right]. \quad (40)$$

The corresponding phase diagram is shown in figure 10, which is again dominated by regions of incommensurate order. The ordering wavevectors in figure 10 refer to the hexagonal basis. As with ...ABAB... stacking the results are non-trivial and qualitatively different from the results for ...AAA... stacking. Here again the strength of J_3 is important.

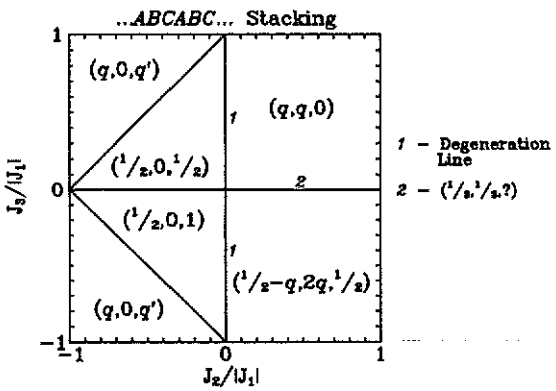

Figure 10. The phase diagram, as a function of further neighbour interactions J_2 and J_3, for the triangular lattice with ...ABCABC... stacking and $J_1 < 0$. Along the line labelled 1 the system selects an infinite number of ordering wavevectors which form a degeneration line in q-space. Only along the line labelled 2 does the system select three-sublattice order with $q = (\frac{1}{3}, \frac{1}{3}, q_z)$.

Again three-sublattice order is stable when $J_2 > 0$ and $J_3 = 0$ which is the phase boundary labelled 2 in figure 10. When $J_3 > 0$ the system goes incommensurate with wavevector $q = (q, q, 0)$ where

$$\cos q = (1/12J_2)\left[1 - (1 + 12J_2 + 36J_2^2 - 12J_2J_3)^{1/2}\right]. \quad (41)$$

Degeneration lines of a different nature occur in this lattice when $J_2 = 0$. For small J_3 the lines are spirals along the q_z direction and are not confined to the $q_z = 0$ plane. These degeneration lines have been described in more detail by Rastelli and Tassi (1986, 1987).

The $LiMO_2$ (M = Ni and Co) series of compounds have the ...ABCABC... type stacking of the ...O–Li–O–M–O–Li–O... triangular sheets. Hence both the transition metal and lithium layers are stacked in the rhombohedral fashion. Recent electrochemical and *in situ* x-ray diffraction measurements (Reimers and Dahn 1992) have shown that the lithium ions in Li_xCoO_2 form a superlattice structure at $x = \frac{1}{2}$. The observed lattice distortion in Li_xCoO_2 is consistent with the lattice decoration in figure 3(*b*) which corresponds to an in-plane wavevector $q = (\frac{1}{2}, 0)$. The results of this section should also be applicable to lithium intercalation in Li_xNiO_2 which is currently not as well understood. Both of these materials are currently used as cathodes in high voltage, secondary lithium batteries. $LiNiO_2$ is also of interest because it is believed to be an $S = \frac{1}{2}$ antiferromagnet (Hirakawa *et al* 1985). Again

the Ni^{3+} magnetic moments form a triangular lattice with ...ABCABC... stacking. The highly quantum nature of the spins in this system leads to complications beyond the scope of this paper. Previous workers have considered this system as essentially two-dimensional and have paid little attention to the nature of the stacking. As we have shown here the type of stacking and the strength of the inter-planar interactions can be very important.

4. Summary and conclusions

Using a mean field approach we have calculated the nature of the ordered phases in stacked triangular lattice gases and antiferromagnets. For ...ABAB... and ...ABCABC... stacking of the triangular sheets further neighbour interactions will in most cases stabilize incommensurate long-range order. For lattice gas and Ising spin systems we expect the incommensurate phases to 'lock in' at low temperature and go commensurate. The results show the profound effects of the stacking when inter-plane interactions are non-zero. These phase diagrams provide a useful starting point for more sophisticated approaches such as Monte Carlo and cluster expansions. In particular they show where in the space of interaction parameters one should perform a Monte Carlo simulation. For a given choice of interactions they indicate suitable boundary conditions for simulations and what choice of sublattices are suitable for cluster expansions.

Acknowledgments

We would like to thank B D Gaulin for many useful comments. JNR acknowledges financial assistance in the form of a post-doctoral fellowship from the Natural Sciences and Engineering Research Council of Canada (NSERC). We also thank NSERC for funding a portion of this work under the strategic grants programme.

References

Aeppli G, Bucher E, Broholm C, Kjems J K, Baumann J and Hufnagl J 1988 *Phys. Rev. Lett.* **60** 615
Ashcroft N W and Mermin N D 1976 *Solid State Physics* (Philadelphia, PA: Saunders College) p 76
Blankschtein D, Ma M, Berker A N, Grest G S and Soukoulis C M 1984 *Phys. Rev.* B **29** 5250
Dahn J R and McKinnon W R 1984a *J. Phys. C: Solid State Phys.* **17** 4231
—— 1984b *J. Electrochem. Soc.* **131** 1823
Diep H T 1992 *Phys. Rev.* B **45** 2863
Eibschutz M, Sherwood R C, Hsu F S L and Cox D E 1973 *Magnetism and Magnetic Materials 1972 (AIP Conf. Proc. No 10)* part 1, ed C D Graham Jr and J J Rhyne (New York: American Institute of Physics) p 684
Glinka C J, Minkiewicz V J, Cox D E and Khattak C P 1973 *Magnetism and Magnetic Materials 1972 (AIP Conf. Proc. No 10)* part 1, ed C D Graham Jr and J J Rhyne (New York: American Institute of Physics) p 659
Goldman A I, Shirane G, Aeppli G, Batlogg B and Bucher E 1986 *Phys. Rev.* B **34** 6564
Harris A B, Mouritson O G and Berlinsky A J 1984 *Can. J. Phys.* **62** 915
Hirakawa K, Kadowaki H and Ubokoshi K 1985 *J. Phys. Soc. Japan* **54** 3526
Kim J-J, Yamada Y and Nagai O 1990 *Phys. Rev.* B **41** 4760
Matsubara F and Sakari I 1987a *J. Phys. Soc. Japan* **56** 2666
—— 1987b *J. Phys. Soc. Japan* **56** 4087

McKinnon W R and Haering R R 1983 *Modern Aspects of Electrochemistry* vol 15, ed R E White, J O'M Bockris and B E Conway (New York: Plenum)
Rastelli E and Tassi A 1986 *J. Phys. C: Solid State Phys.* **19** L423
—— 1987 *J. Phys. C: Solid State Phys.* **20** L303
Reimers J N, Berlinsky A J and Shi A-C 1991 *Phys. Rev.* B **43** 865
Reimers J N and Dahn J R 1992 *J. Electrochem. Soc.* **139** 2091
Solin S A 1982 *Advances in Chemical Physics* vol 49, ed I Prigogine and S A Rice (New York: Wiley) p 455
Villain J, Bidaux R, Carton J P and Conte R 1980 *J. Physique* **41** 1263
Wannier G H 1950 *Phys. Rev.* **79** 357
Whittingham M S 1978 *Prog. Solid State Chem.* **12** 41